https://doi.org/10.5194/hess-2024-274
Preprint. Discussion started: 23 September 2024

Hydrology and Earth System Sciences
Discussions
Open Access
EGU

Influence of Spatial Heterogeneity of Runoff Generation on the Distributed Unit Hydrograph for Flood Prediction

Bin Yi[1,2], Lu Chen[1,2,3]*, Binlin Yang[1,2], Zhiyuan Leng[1,2], Siming Li[1,2], Tao Xie[1,2]

1. *School of Civil and Hydraulic Engineering, Huazhong University of Science and Technology, Wuhan, 430074, China*

2. *Hubei Key Laboratory of Digital Valley Science and Technology, Wuhan 430074, China*

3. *School of Water Resources and Civil Engineering, Tibet Agricultural & Animal Husbandry University, Linzhi 860000, China*

Correspondence: Lu Chen (chen_lu@hust.edu.cn)

Abstract: The spatial scale mismatch between runoff generation and runoff routing is an acceptable compromise but a common issue in hydrological modeling. Moreover, there is hardly any report available on whether a unit hydrograph (UH) that is consistent with the spatial scale of runoff generation can be computed. The objective of this study was to explore the influence of spatial heterogeneity of runoff generation on the UH for flood prediction. To this end, a novel GIS-based dynamic time-varying unit hydrograph (DTDUH) was proposed based on the time-varying unit hydrograph (TDUH). The DTDUH can be defined as a typical hydrograph of direct runoff which gets generated from one centimeter of effective rainfall falling at a uniform rate over the saturated drainage basin uniformly during a specific duration. The DTDUH was computed based on the saturated areas of the watershed instead of the global watershed. The saturated areas were extracted based on the TWI. Finally, the Longhu River basin and Dongshi River basin were selected as two case studies. Results showed that the proposed method exhibited consistent or better performance compared with that of the linear reservoir routing method, and performed better than the TDUH method. The proposed method can be used for watersheds with sparse gauging stations and limited observed rainfall and runoff data, as for the TDUH method. Simultaneously, it is well applicable to humid or mountain watershed where

https://doi.org/10.5194/hess-2024-274
Preprint. Discussion started: 23 September 2024

saturation-excess rainfall is dominant.

Keywords: Hydrological modeling; Distributed unit hydrograph; Runoff routing; Runoff generation; XAJ model

1. Introduction

The assumption that basins behave as linear systems (i.e., there is proportionality and additivity between excess rainfall and total storm response) has been the core of hydrology over the past century (Goodrich et al., 1997; Bunster et al., 2019). On such conditions, a single response function named the UH has been widely applied to acquire the stormflow at the basin outlet (Czyzyk et al., 2020). The UH can be developed for both gauged and ungauged watersheds (Monajemi et al., 2021). For gauged basins, unit hydrographs are derived from observed data by measuring rainfall and runoff data. For ungauged basins, some synthetic methods, such as Snyder's method (Snyder, 1938) and Gray's method (Gray, 1961), are used to determine the unit hydrographs from spatially averaged basin characteristics. One variation is the synthetic UH method proposed by Clark (1945), in which the UH was derived by integrating two basic features of a watershed rainfall-runoff process. Specifically, translation through water movement was characterized by the time-area method, and linear reservoir routing was used to represent attenuation through storage (Cho et al., 2018; Bunster et al., 2019). This history of development was synthesized in the works of Rodríguez-Iturbe and Valdés (1979) and Gupta et al. (1980), who proposed the geomorphological instantaneous unit hydrograph (GIUH). Subsequently, the width function-based geomorphological instantaneous unit hydrograph (WFIUH) method has been formulated with the development of digital elevation models (DEMs) and geographic information system (GIS) technology (Seo et al., 2016). The WFIUH was derived by combining the flow paths to

https://doi.org/10.5194/hess-2024-274
Preprint. Discussion started: 23 September 2024


Hydrology and Earth System Sciences
Discussions

the outlet given by the width function with the flow celerity along the flow paths (Kirkby, 1976).

The UH method assumes the watershed response to efficient rainfall to be linear and time-invariant, and rainfall to be spatially homogeneous. In contrast to the linearity assumption, basins have been shown to exhibit nonlinearity in the transformation of excess rainfall to stormflow (Bunster et al., 2019). For a small watershed, Minshall (1960) showed that significantly different UHs were produced by different rainfall intensities. To cope with this nonlinearity, Rodríguez-Iturbe et al. (1982) extended the GIUH to the geomorphoclimatic IUH (GcIUH) by incorporating excess rainfall intensity. Lee et al. (2008) proposed a variable kinematic wave GIUH accounting for time-varying rainfall intensity, which may be applicable to ungauged catchments that are influenced by the high intensity of rainfall. To this end, it is necessary to consider the geomorphic characteristics of the watershed and incorporate time-varying rainfall intensity in the rainfall-runoff modeling processes.

Spatially distributed travel time models, also known as Spatially Distributed Unit Hydrograph models (DUH) (Maidment et al., 1996), are a semi-analytical form of the WFIUH identified by Rigon et al. (2016) in which spatially distributed flow celerity associated with the watershed characteristics and temporally varying excess rainfall rates can be considered. In this method, the travel time of each grid cell can be calculated by dividing the travel distance of a cell to the next cell by the velocity of flow generated in that cell (Paul et al., 2018). The travel time is then summed along the flow path to obtain the total travel time from each cell to the outlet. The DUH is thus derived using the distribution of travel time from all grid cells in a watershed. Several aspects (i.e. Rainfall intensities, upstream contributions, watershed equilibrium) have attracted much attention to obtain more accurate travel time distributions. Some DUH methods assumed a time-invariant travel time field and ignored the

https://doi.org/10.5194/hess-2024-274
Preprint. Discussion started: 23 September 2024


Hydrology and Earth System Sciences
Discussions

dependence of travel time on excess rainfall intensity (Melesse and Graham, 2004; Noto and La Loggia, 2007; Gibbs et al., 2010; Grimaldi et al., 2010), while others suggested various UHs corresponding to different storm events, namely time-varying distributed unit hydrograph (TDUH) (Martinez et al., 2002; Sarangi et al., 2007; Du et al., 2009). The upstream contributions to the travel time estimation should also be considered in the time-varying DUH method, which was developed from a static upstream contribution to a dynamic contribution. For example, Bunster et al. (2019) developed a TDUH model that accounts for dynamic upstream contributions and compared its performance against other TDUH methods, and characterized the temporal behavior of upstream contributions and its impact on travel times in the basin. However, the methods discussed above assumed that equilibrium in each individual grid cell or global watershed can be reached before the end of the rainfall excess pulse. To this end, Yi et al. (2022) proposed a time-varying distributed unit hydrograph method for runoff routing that accounts for dynamic rainfall intensity and soil moisture content, namely the time-varying distributed unit hydrograph considering soil moisture content (TDUH-MC). Hydrologists have made great efforts to address the nonlinear issues of the UHs in the past decades, while these approximations are still acceptable compromises in challenging hydrology research.

Nevertheless, we found that the approximations discussed above neglected the influence of spatial heterogeneity of runoff generation on the UH. For instance, in a humid watershed, the excess rainfall can be more inclined to happen in near-channel areas, and sometimes in the arid zones with long storms durations according to the saturation-excess mechanism (Li and Sivapalan, 2014). In previous studies, the time-varying rainfall intensities were commonly considered to obtain more accurate travel time distributions to compute the UH for the whole basin, while the depth of the excess rainfall was also

https://doi.org/10.5194/hess-2024-274
Preprint. Discussion started: 23 September 2024


Hydrology and Earth System Sciences
Discussions

87 considered to be uniformly distributed throughout the whole watershed (the excess rainfall comes from
88 local saturated areas). The outflow hydrograph is then calculated by superimposing the response to
89 each excess rainfall pulse, or equivalently by convoluting the spatially averaged excess rainfall and a
90 UH obtained from the IUH. This raised the question of whether the unit hydrograph can reflect the
91 realities of the runoff routing processes of an actual watershed.

92 The problem of spatial scale mismatch between runoff generation and confluence theory is
93 prevalent in hydrological modeling, and hydrologists almost ignore the forecasting errors associated
94 with this issue. For example, the Xinanjiang (XAJ) model is a conceptual hydrological model proposed
95 by Zhao et al. (1980) for flood forecasts in the Xin'an River basin. It has been widely used in humid
96 and semi-humid watersheds all over the world (Zhao, 1992; Zhou et al., 2019; Huang et al., 2020). In
97 the model, two parabolic curves are adopted to represent the spatially non-uniform distribution of the
98 tension water storage and the free water storage. To match the spatial scales of the runoff generation
99 and the runoff routing, the excess rainfall generated in the saturated areas was assumed to be uniformly
100 distributed across the whole basin. However, this assumption may result in huge errors, and there is
101 hardly any report available on whether UH that is consistent with the spatial scale of runoff generation
102 can be computed (Andrieu et al., 2021).

103 The objective of this study was therefore to explore the influence of spatial heterogeneity of runoff
104 generation on the UH for flood prediction. The main contributions of the present study are given as
105 follows. 1) The DUH method was used as the basic tool to compute the DTDUH corresponding to
106 various saturated states of the watershed. 2) The definition of the DTDUH was different from the
107 traditional TDUH as it represented the characteristics of the runoff-generating areas instead of the

https://doi.org/10.5194/hess-2024-274
Preprint. Discussion started: 23 September 2024


Hydrology and Earth System Sciences
Discussions

whole basin. 3) The XAJ model was used as the hydrological modeling framework to compare the performances of TDUH and DTDUH based on flood events. The Longhu River basin and the Dongshi River basin in the Guangdong Province, China, were selected as two case studies. The influence of spatial heterogeneity of runoff generation on the UH for flood prediction was investigated.

The remaining chapters of this paper are arranged as follows: In Hydrological models, the processes of DTDUH considering the spatial heterogeneity of runoff generation are introduced, and the parameter calibration method, evaluation criteria as well as the hydrologic model are demonstrated. In section study area and data, the rainfall and runoff data and the study areas are described. In section results, the performances and results of the TDUH and DTUHD are compared. In section discussion, the results and methods were discussed and in section conclusions, relevant conclusions were drawn.

2. Hydrological models

2.1 Runoff generation based on the saturation-excess mechanism

Mostly, saturation-excess runoff is the major runoff mechanism in humid areas (Tromp-Van Meerveld and McDonnell, 2006; Hoang et al., 2017). Many hydrological models, such as the TOPMODEL (Beven and Kirkby, 1979), the Variable Infiltration Capacity (VIC) model (Liang et al., 1994), the Probability Distributed Model (PDM) (Moore, 2007), the XAJ model (Zhao, 1992), and the Australian Water Balance Model (Boughton, 2004), simulate saturation-excess runoff by introducing a statistical distribution of tension water storage capacity using different methods. Simultaneously, a free water capacity distribution curve is usually used to divide the total runoff into the surface runoff, interflow, and groundwater. In the XAJ model, two parabolic curves are adopted to represent the spatially non-uniform distribution of the tension water storage and free water storage (Fig. 1).

https://doi.org/10.5194/hess-2024-274
Preprint. Discussion started: 23 September 2024

Hydrology and Earth System Sciences
Discussions

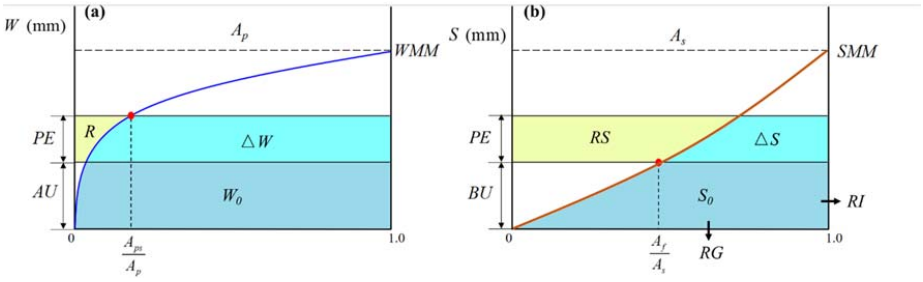

Figure 1. (a) Tension water storage capacity curve, and (b) Free water storage capacity curve

The difference between field capacity and total soil water content is defined as tension water storage capacity, the maximum amount of water available in an unsaturated zone. In the XAJ model, a tension water capacity curve is introduced (Fig. 1(a)) to describe the non-uniform distribution of tension water capacity throughout the basin or sub-basin. In Fig. 1(a), A_{ps} is the partial pervious area where the tension water storage capacity is less than or equal to the value W, which is the tension water capacity at a point, varying from 0 to a maximum WMM; A_p is the pervious area; W_0 is the initial areal mean tension water storage (mm); and AU is the vertical coordinate corresponding to W_0. The functional relationship of the tension water storage capacity curve is expressed as:

$$\frac{A_{ps}}{A_p} = 1 - \left(1 - \frac{W}{WMM}\right)^B \tag{1}$$

Based on Eq. (1), when rainfall exceeds evaporation, the runoff generated in the saturated areas can be calculated as:

$$R = \begin{cases} \int_{AU}^{AU+PE} \frac{A_{ps}}{A_p} dW & PE + AU < WMM \\ PE - WM + W_0 & PE + AU \geq WMM \end{cases} \tag{2}$$

The total runoff R (R=RS+RI+RG), generated in a wet period in accordance with Eq. (2), must be separated into three components, including the surface runoff, the subsurface stormflow, and the

https://doi.org/10.5194/hess-2024-274
Preprint. Discussion started: 23 September 2024


Hydrology and Earth System Sciences
Discussions

surface runoff. Thus, the concept of free water storage capacity was used, and it was assumed to be distributed between zero and a point maximum *SMM* in a parabolic manner, as shown in Fig. 1(b). In Fig. 1(b), A_p is the pervious area of the catchment; A_f is the area where the free water storage capacity is less than or equal to the value *S*, varying from 0 to *SMM*; A_s is the runoff generation area; S_0 is the initial areal mean free water storage (mm); *BU* is the vertical coordinate corresponding to S_0; and *RI*, *RG* represent the depth of the interflow and subsurface flow. The functional relationship of the free water storage capacity curve is expressed as:

$$\frac{A_f}{A_s} = 1 - \left(1 - \frac{S}{SMM}\right)^{EX} \tag{3}$$

The total runoff *R*, generated in a wet period in accordance with Eq. (3), can be subsequently separated into three components, including the surface runoff, interflow, and groundwater, which can be expressed by

$$RS = \begin{cases} FR\int_{BU}^{BU+PE} \frac{A_f}{A_s} dS & PE + BU < SMM \\ FR\left(PE + S_0 - SM\right) & PE + BU \geq SMM \end{cases} \tag{4}$$

$$RI = KI \cdot FR \cdot \int_0^{BU} \frac{A_f}{A_s} dS \tag{5}$$

$$RG = KG \cdot FR \cdot \int_0^{BU} \frac{A_f}{A_s} dS \tag{6}$$

where *RS*, *RI*, and *RG* represent the depth of the surface runoff, interflow, and groundwater respectively (mm); *FR*, equaling to *R*/*PE*, is the proportion of the runoff-producing area over the whole basin; *SM* is the areal mean free water capacity (mm); and *KI* and *KG* are outflow coefficients of the free water storage to interflow and groundwater, respectively.

https://doi.org/10.5194/hess-2024-274
Preprint. Discussion started: 23 September 2024

Hydrology and Earth System Sciences
Discussions

2.2 Definition, conceptual and derivation of the DTDUH

The GIS-derived DUH method was employed for the surface runoff routing calculations, which allowed the velocity to be calculated on a grid cell basis over the watershed. To remove the linearity assumption, fully distributed models use routing methods which are usually computationally intensive because they solve the St. Venant equations (Bunster et al., 2019), so they are usually limited to small basins. Therefore, the DUH method is an alternative method that allows the use of distributed information in a much more efficient manner. The TDUH method was used for the computation of the UH, which considered both the time-varying rainfall intensities and the soil moisture. More details can be found in Yi et al. (2022). The DTDUH proposed in this study is computed based on the TDUH, and the proposed DTDUH was computed based on the runoff generation areas instead of the whole basin. This realization was significantly different from the current understanding (Gibbs et al., 2010; Goñi et al., 2019; Andrieu et al., 2021). The differences in the definition and assumptions between the current theory and the DTDUH have been concluded in Table 1, and the schematic diagram of the DTDUH method is shown in Fig. 2.

Table 1. The differences in the definition and assumptions between the current theory and the DTDUH.

Differences	Current theory	DTDUH
Definition	A typical hydrograph of direct runoff which gets generated from one centimeter of effective rainfall falling at a uniform rate over the entire drainage basin uniformly during a specific duration.	A typical hydrograph of direct runoff which gets generated from one centimeter of effective rainfall falling at a uniform rate over the saturated drainage basin uniformly during a specific duration.
Assumption	i) The effective rainfall is uniformly distributed over the entire drainage basin. ii) The effective rainfall occurs uniformly within its specifier duration.	i) The effective rainfall is uniformly distributed over the saturated drainage areas. ii) The effective rainfall occurs uniformly within its specifier duration.

https://doi.org/10.5194/hess-2024-274
Preprint. Discussion started: 23 September 2024

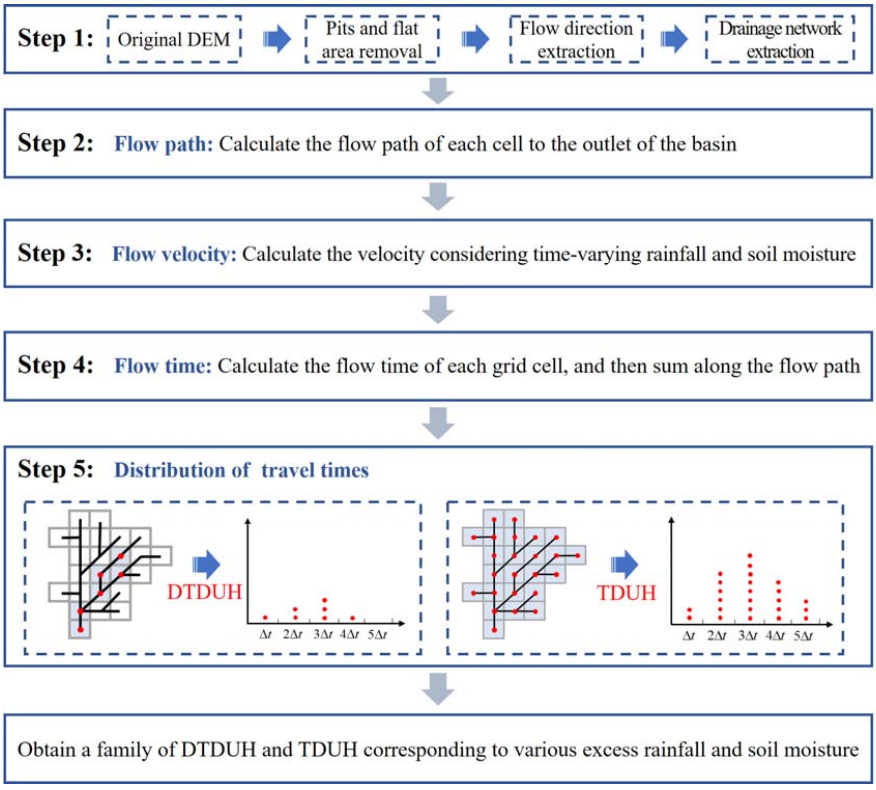

Figure 2. Schematic diagram of the DTDUH method. The main differences between the DTDUH and TDUH lie in that the DTDUH is computed based on local areas while the TDUH is for the global watershed.

1) The drainage network can be identified based on the advanced DEM preprocessing method (Grimaldi et al., 2012). Then, the flow path collection ($\mathbf{Road}_{A_j}$) of each gird cell A_j along the flow directions to the basin outlet can be created. For the whole basin, the flow path collection of all the grid cells ($\mathbf{Road}$) is expressed by

$$\mathbf{Road} = \left\{ \mathbf{Road}_{A_j} \middle| A_j \in \mathbf{A} \right\} \tag{7}$$

where A_j ($j = 1, 2, \cdots, N$) is the total number of grid cells, N is the total grid cells of the basin; and $\mathbf{A}$ is the collection of all the grid cells.

https://doi.org/10.5194/hess-2024-274
Preprint. Discussion started: 23 September 2024


Hydrology and Earth System Sciences
Discussions

189 The XAJ model adopted the saturation excess runoff generation mechanism, that is, there is no
190 runoff generated until the tension water capacity is satisfied. However, current methods compute the
191 DUH corresponding to the whole basin. To this end, we proposed to create a collection of flow paths
192 for the saturated areas, and the specific formula is given by

193 $$\mathbf{Road}_{\alpha} = \left\{ \mathbf{Road}_{A_j} \middle| A_j \in \mathbf{A}_{\alpha} \right\} \tag{8}$$

194 where $\mathbf{Road}_{\alpha}$ ($\mathbf{Road}_{\alpha} \subseteq \mathbf{Road}$) is the flow path collection of the saturated grid cells when the soil
195 moisture proportion is α; and $\mathbf{A}_{\alpha}$ is the collection of the saturated grid cells when the soil moisture
196 proportion is α.

197 2) The flow velocity of each grid cell corresponding to the collection $\mathbf{Road}_{\alpha}$ is computed based
198 on the watershed characteristics and the spatial-temporal distribution characteristics of rainfall and soil
199 moisture, and the specific formula is given as Eq. (9) (Yi et al., 2022).

200 $$V = k \cdot S^{\frac{1}{2}} \cdot \left(\frac{I_t}{I_c} \right)^{\frac{2}{5}} \cdot (\theta_t)^{\gamma} \tag{9}$$

201 where V (m s^{-1}) is the flow velocity; k (m s^{-1}) is the land use or flow type coefficient, S (m m^{-1}) is the
202 slope of the grid cell; I_t (mm h^{-1}) is the excess rainfall intensity at time t; I_c is the reference excess
203 rainfall intensity of the basin; γ (unitless) is an exponent smaller than unity, which represents the
204 nonlinear relationship between soil moisture content and flow velocity; and θ_t (unitless) represents the
205 soil moisture content of the unsaturated areas at time t, which can be calculated based on Eq. (10)
206 referring to Yi et al (2022)

207 $$\theta_t = \frac{(B+1)W_t}{WMM + B \cdot W_t} \tag{10}$$

208 3) The travel time for each grid cell in collection $\mathbf{Road}_{\alpha}$ can be calculated by Eq. (11). To

https://doi.org/10.5194/hess-2024-274
Preprint. Discussion started: 23 September 2024


Hydrology and Earth System Sciences
Discussions

compute the total travel time τ_i of flow from each cell i to the outlet, travel times along the R_i cells belonging to the flow path that starts at that cell are added based on Eq. (12).

$$\Delta\tau_j = \frac{L_j}{V} \quad \text{or} \quad \Delta\tau_j = \frac{\sqrt{2}L_j}{V} \tag{11}$$

$$\tau_j = \sum_{A_j \in \mathbf{A}_\alpha} \Delta\tau_j \tag{12}$$

where $\Delta\tau_j$ is the retention time in grid cell A_j; τ_j is the total travel time along the flow path for grid cell A_j; L_j is the grid cell size. When the rasterized flow is flowing along the edges of the grid cell, the travel length is the cell size L_j, whereas the travel length is $\sqrt{2}L_j$ when it is flowing diagonally.

4) Develop a cumulative travel time map of the saturated areas instead of the whole basin based on cell-by-cell estimates for hillslope velocities. The cumulative travel time map is further divided into isochrones, which can be used to generate a time-area curve and the resulting DTDUH corresponding to the collection $\mathbf{Road}_\alpha$ instead of $\mathbf{Road}$.

Specifically, the DTDUH was computed considering the time-varying characteristics of the saturated areas, and the excess rainfall was redistributed in the saturated areas instead of the whole basin. The diagram of the DTDUH derivation processes corresponding to various saturated soil moisture can be shown in Fig. 3. The total travel time from each saturated grid cell to the outlet is obtained by directly recording each particle's total travel time from the initial location until the particle leaves the basin. We can obtain the DTDUH when the last particle leaves the basin. There are 24 grid cells in the basin. For instance, the derivation of the TDUH corresponding to saturated proportions 25% (6 grid cells) is shown in Fig. 3(a). The DTDUH is not the same as the TDUH until the basin reaches a global saturation as Fig. 3(d). For instance, when there occurs a stormflow with a depth of 10 mm in the whole basin and the saturated proportion is 50%, the actual depth of the excess rainfall in the

https://doi.org/10.5194/hess-2024-274
Preprint. Discussion started: 23 September 2024

Hydrology and Earth System Sciences
Discussions

230 saturated area is 20 mm. In tradition, the flow hydrograph was calculated using the TDUH as Fig. 3(d),
231 neglecting the issue that excess rainfall particles are only in the saturated areas. This neglect therefore
232 leads to errors because the unsaturated areas where no excess rainfall is generated contribute to the
233 confluence. To solve this issue, the flow hydrograph was calculated using the DTDUH as Fig. 3(b) in
234 this study, and in turn, could improve the forecast performances of the hydrological model.

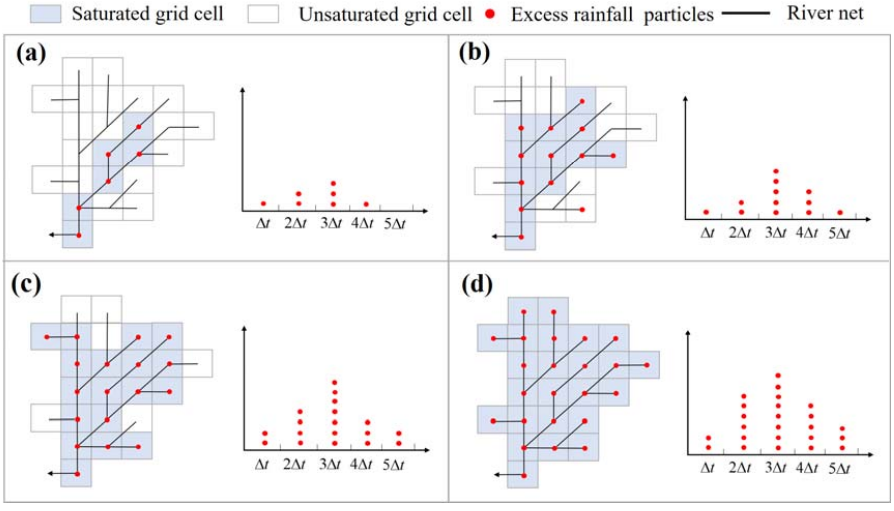

235

236 **Figure 3.** The diagram of the DTDUH corresponds to various soil moisture. (a) $\alpha_s = 0.25$. (b)
237 $\alpha_s = 0.50$. (c) $\alpha_s = 0.75$. (d) $\alpha_s = 1.00$.

238 *2.3 Hydrological modeling framework*

239 The XAJ model proposed by Zhao et al. (1980) was used as the hydrological modeling framework.
240 It has been widely used in humid and semi-humid watersheds all over the world. There are four
241 modules in the model including the evapotranspiration module, runoff generation module, runoff
242 partition module, and runoff routing module. For the evapotranspiration module, the soil profile of
243 each sub-basin is divided into three layers, the upper, lower, and deeper layers, and only when water

https://doi.org/10.5194/hess-2024-274
Preprint. Discussion started: 23 September 2024

Hydrology and Earth System Sciences
Discussions

244 in the layer above it has been exhausted does evaporation from the next layer occur. For the runoff
245 generation and runoff partition modules in the XAJ model, they have been reviewed in Section 2.1.
246 Finally, for the runoff routing module, subsurface stormflow and subsurface runoff were considered
247 using a free reservoir. To investigate the influence of spatial heterogeneity of runoff generation on the
248 runoff routing, linear reservoir, TDUH, and DTDUH were selected as the surface runoff routing
249 methods. When the watershed is divided into multiple sub-basins, the Muskingum method will be used
250 to confluence the runoff of each sub-basin to the outlet of the basin. The XAJ modeling framework
251 used in this study is given in Fig. 4.

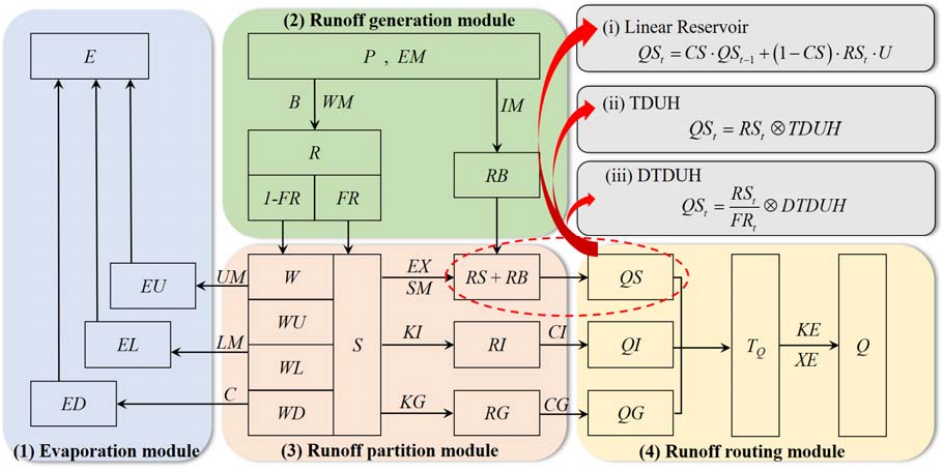

252

253 **Figure 4.** Schematic diagram of the XAJ model.

254 The depths of the surface runoff calculated by Eq. (4) are obtained after a redistribution to the
255 whole basin. As a matter of fact, the depths of the surface runoff should be calculated only over the
256 saturated areas when the DTDUH was selected as the surface runoff routing method, which can be
257 expressed by

258 $$RS_s^{'} = \frac{RS_s}{FR} \tag{13}$$

https://doi.org/10.5194/hess-2024-274
Preprint. Discussion started: 23 September 2024


Hydrology and Earth System Sciences
Discussions

where $RS_s^{'}$ is the depth of the surface runoff corresponding to the saturated areas.

When the linear reservoir, TDUH, and DTDUH were used respectively for the surface runoff routing, the flow discharge at the outlet of the watershed can be computed by

$$QS_t = CS \cdot QS_{t-1} + (1 - CS) \cdot RS_t \cdot \frac{F}{3.6\Delta t} \tag{14}$$

$$QS_t = RS_t \otimes TDUH \tag{15}$$

$$QS_t = RS_t^{'} \otimes DTDUH \tag{16}$$

where CS is the recession constant of the surface water storage; F (km^2) is the area of the basin, and $\otimes$ is the symbol of convolution.

Simultaneously, the subsurface stormflow (RI) and subsurface runoff (RG) were considered using a free reservoir, and the proposed routing schemes are applied only to RS. Their expressions are given by

$$QI_t = CI \cdot QI_{t-1} + (1 - CI) \cdot RI_t \cdot U \tag{17}$$

$$QG_t = CG \cdot QG_{t-1} + (1 - CG) \cdot RG_t \cdot U \tag{18}$$

Subsequently, the total runoff (Q_t) at the outlet of the basin can be calculated by

$$Q_t = QS_t + QI_t + QG_t \tag{19}$$

2.4 Model calibration and evaluation

The Shuffled Complex Evolution Algorithm (SCE-UA) technique was developed by the University of Arizona in 1992 for nonlinear, high-dimensional optimization issues (Duan et al., 1992). The technique has been used extensively for calibrating hydrological models (Zhou et al., 2019). Consequently, the SCE-UA method was employed in this study to optimize the parameters of the hydrological model. An aggregated objective function made up of three measures was used for the parameter calibration (Brunner et al., 2021; Yi et al., 2022; Yi et al., 2023). The aggregated objective

https://doi.org/10.5194/hess-2024-274
Preprint. Discussion started: 23 September 2024


Hydrology and Earth System Sciences
Discussions

function and three metrics are expressed by

$$E_{\mathrm{NS}}=1-\frac{\sum_{t=1}^{T}\left|Q_s^t-Q_o^t\right|}{\sum_{t=1}^{T}\left|Q_o^t-\overline{Q_o}\right|} \tag{20}$$

$$E_{\mathrm{KG}}=1-\sqrt{(r-1)^2+\left(\frac{\sigma_s}{\sigma_o}-1\right)^2+\left(\frac{\mu_s}{\mu_o}-1\right)^2} \tag{21}$$

$$R_{\mathrm{SR}}=\sqrt{\frac{\sum_{t=1}^{T}\left(Q_o^t-Q_s^t\right)^2}{\sum_{t=1}^{T}\left(Q_o^t-\overline{Q_o}\right)^2}} \tag{22}$$

$$M=0.5\times\left(1-E_{\mathrm{NS}}\right)+0.25\times\left(1-E_{\mathrm{KG}}\right)+0.15\times\left(1-\log\left(E_{\mathrm{NS}}\right)\right)+0.1\times R_{\mathrm{SR}} \tag{23}$$

where Q_o^t is the observed discharge at time t; Q_s^t is the simulated discharge at time t; $\overline{Q_o}$ is the mean of the observed discharge; T is the duration of the flood event; r is the correlation coefficient between the observed and simulated flood; σ_s and σ_o are the standard deviation values for the simulated and observed responses, respectively; and μ_s and μ_o are the corresponding mean values.

Several criteria were used for the model performance evaluation, consisting of the E_{NS}, the Root Mean Square Error (*RMSE*), the relative flood peak error (Q_{P}), and the flood peak time error (T_{P}), which can be expressed by

$$RMSE=\sqrt{\frac{1}{T}\sum_{t=1}^{T}\left(Q_s^t-Q_o^t\right)^2} \tag{24}$$

$$Q_p=\frac{Q_p^s-Q_p^o}{Q_p^o} \tag{25}$$

$$T_p=T_p^s-T_p^o \tag{26}$$

where Q_p^s is the simulated flood peak discharge; Q_p^o is the observed flood peak discharge; T_p^o is the observed flood peak time; and T_p^s is the simulated flood peak time.

The parameters of the XAJ model and the DTDUH method were calibrated or evaluated, respectively. An explanation of different parameters for evaluation and calibration is summarized in Table 1.

https://doi.org/10.5194/hess-2024-274
Preprint. Discussion started: 23 September 2024

Hydrology and Earth System Sciences
Discussions

301 **Table 1**. Explanation of different parameters for evaluation and calibration.

Description	Notation	Explanation
Ratio of potential evapotranspiration to pan evaporation	*KC* (unitless)	15 parameters of the XAJ model, and these parameters are calibrated based on the SCE-UA method. (*KE and XE are required when a watershed is divided into several sub-basins*)
Averaged soil moisture storage capacity of the upper layer	*UM* (mm)	
Averaged soil moisture storage capacity of the lower layer	*LM* (mm)	
Averaged soil moisture storage capacity of the deep layer	*DM* (mm)	
Exponential of the distribution to tension water capacity	*B* (unitless)	
Percentage of impervious in the watershed	*IM* (unitless)	
Evapotranspiration coefficient of the deeper layer	*C* (unitless)	
Mean free water capacity of the surface soil layer	*SM* (mm)	
Exponent of the distribution to free water capacity	*EX* (unitless)	
Outflow coefficients of the free water storage to subsurface stormflow	*KI* (unitless)	
Outflow coefficients of the free water storage to subsurface flow	*KG* (unitless)	
Recession constants of the subsurface stormflow	*CI* (unitless)	
Recession constants of the surface runoff storage	*CG* (unitless)	
Recession constants of channel network storage	*CS* (unitless)	
Muskingum time constant	*KE* (h)	
Muskingum weighting factor	*XE* (unitless)	
Lag in time	*L* (h)	
Reference rainfall intensity	I_c (mm/h)	Evaluated based on the average rainfall intensity
Power law related to the influence of soil moisture on flow velocity	γ (unitless)	Evaluated based on the average rainfall intensity (Yi et al., 2022)
Slope of the watershed grid cell	*S* (m/m)	Evaluated based on DEM of the watershed
Land use or flow type coefficient	*k* (m/s)	Evaluated based on different underlying surface types or different flow states (Ajward and Muzik, 2000)

302 ## 3. Study area and data

303 The Longhu River basin and the Dongshi River basin were selected as two case study watersheds.

https://doi.org/10.5194/hess-2024-274
Preprint. Discussion started: 23 September 2024

Hydrology and Earth System Sciences
Discussions
Open Access
EGU

304 The Longhu River and the Dongshi River are located in the humid mountain area, which originates
305 from the Hanjiang River basin of the Guangdong Province, China. The Longhu River is 17.4 km long,
306 with a basin area of 102.7 km^2, and the mean slope of the basin is 2.9 ‰. The Dongshi River is 23.6 km
307 long, with a basin area of 152.4 km^2, and the mean slope of the basin is 3.56 ‰. The DEM data of the
308 two basins were collected from Geospatial Data Cloud (http://www.gscloud.cn/). The land cover data
309 can be accessed from Tsinghua University (http://data.ess.tsinghua.edu.cn/). The distributions of the
310 DEM, slope, and land cover for the two basins are shown in Fig. 5.

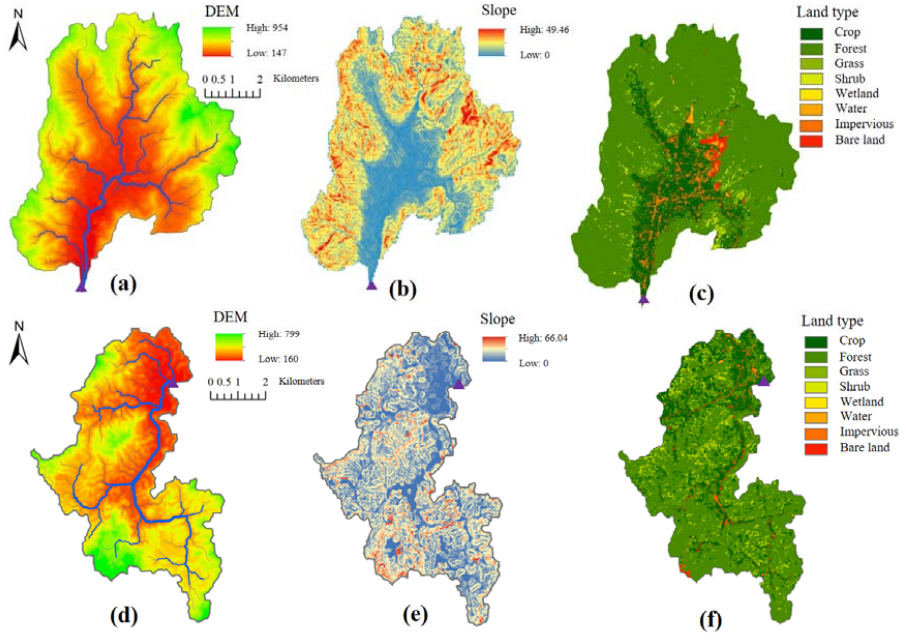

311

312 **Figure 5.** Distribution of the DEM, slope, and land cover. (a), (b) and (c) are the DEM, slope, and land
313 cover corresponding to the Dongshi River basin. (d), (e) and (f) are the DEM, slope, and land cover
314 corresponding to the Longhu River basin.

315 Additionally, the rainfall and evaporation data from meteorological stations for the two basins

https://doi.org/10.5194/hess-2024-274
Preprint. Discussion started: 23 September 2024

Hydrology and Earth System Sciences
Discussions

were collected from 1973 to 2020, and the simultaneous hourly runoff data for the outlet of the watersheds were collected as well, and the data were collected from Meizhou Hydrological Bureau. A total of 16 isolated storms were identified from the continuous flow process in the Longhu and Dongshi River basins, respectively. The Dongshi hydrological station was built in recent years, and the flow sequences were therefore short. Specifically, 16 flood events in the Longhu River basin with 1 hour interval were collected from 1973 to 2016, and 16 flood events with 1 hour interval were collected from the Dongshi River basin from 2015 to 2020. The statistics of these flood events are shown in Table 2, where 12 flood events were used to calibrate the model, and 4 flood events were used for verification for the two basins. The average flood peaks for the Longhu River basin and the Dongshi River basin are 116.7 $m^3 s^{-1}$ and 73.0 $m^3 s^{-1}$, respectively. The average flood durations are about 30 h and 33 h, respectively. Moreover, to consider the initial condition, the antecedent precipitation was calculated based on the daily recession coefficient of the water storage.

Table 2. Statistics of the flood events in the Longhu and the Dongshi River basins.

Watershed	Periods	Flood events	Rainfall (mm)	Flood peak (m^3 s^{-1})	Time duration (h)
Longhu	Calibration	19730508	80.0	94.5	27
		19730720	76.7	180.0	17
		19750526	54.9	101.0	21
		19760702	73.0	137.0	28
		19770526	73.8	90.4	18
		19771003	62.1	97.5	19
		19790607	100.3	93.4	24
		19890502	46.5	132.0	29
		20030517	94.0	140.0	46
		20060601	56.0	96.5	37
		20120527	118.8	128.0	27
		20130713	214.4	228.0	30
	Verification	20150601	83.4	85.0	44
		20150831	102.6	83.2	30

https://doi.org/10.5194/hess-2024-274
Preprint. Discussion started: 23 September 2024

Hydrology and Earth System Sciences
Discussions

		20160430	111.2	91.0	54
		20160903	85.4	89.7	26
Dongshi	Calibration	20150509	105.2	62.9	38
		20150721	132.0	82.0	29
		20160811	90.0	51.3	48
		20160819	112.5	34.9	19
		20161021	158.8	48.0	49
		20170501	84.5	98.3	22
		20170515	84.0	43.7	29
		20170613	139.2	37.2	31
		20170929	71.0	101.2	25
		20180606	61.5	34.9	32
		20180702	23.5	44.3	25
		20190418	86.4	35.5	18
	Verification	20190609	107.6	272.0	27
		20190612	74.0	100.0	66
		20200522	67.5	71.0	37
		20200607	109.3	50.6	26

4. Results

4.1 Calibration of parameters

The core of the DUH was the calculation of the grid flow velocity. The parameters that need to be determined in Eq. (9) consist of k, S, I_c, and γ, in which k was the velocity coefficient and was determined based on different underlying surface types or different flow states (Foda et al., 2017), as shown in Fig. 5(c) and Fig. 5(f). S was the grid cell slope of the study areas, which could be obtained from the DEM data of the target basin, as shown in Fig. 5(b) and Fig. 5(e). I_c was determined using the hourly mean rainfall intensity of the target basin, and this parameter was 10 mm h^{-1} for the two study watersheds. Additionally, γ is a power law related to the influence of soil moisture on flow velocity, and the sensitivity analysis for variable gamma has been made in the previous study. The results show that the mean flow velocity of the basin was significantly influenced by exponent γ. In addition, when the soil moisture content exceeded 0.7, the variation range of mean flow velocity decreased sharply, which means that the influence of parameter γ on the flow velocity decreased

https://doi.org/10.5194/hess-2024-274
Preprint. Discussion started: 23 September 2024


Hydrology and Earth System Sciences
Discussions

342 gradually with the increase of soil moisture content. In theory, I_c and γ are different from one flood
343 event to another. However, it is difficult to realize in practical use, and we usually adopted the unit
344 hydrograph charactering the average physical properties of a watershed. Thus, in practical flood
345 forecasting, the parameter γ should be a constant once it is determined. This is similar to the influence
346 of upstream contributions to the flow velocity formula in previous research (Rodríguez-Iturbe et al.,
347 1992). Therefore, the parameter γ of soil moisture content was determined to be 0.5 to reflect the
348 influence of soil moisture content on the flow velocity for the two basins (Yi et al., 2022). In addition,
349 it is noteworthy that the raster size of the two basins was divided into 30 m × 30 m. The rationality of
350 the TDUH in these two basins had been validated in our previous research (Yi and Chen, 2022; Yi et
351 al., 2022), and thus was not calibrated in this study.

352 *4.2 Computation of the DTDUH*

353 The TDUH was derived referring to Yi et al. (2022) and the rationality of the TDUH has been
354 validated. The derivations of the proposed DTDUH were similar to those of the TDUH. The main
355 difference lay that the DTDUH was derived for a specific saturated area. To obtain the DTDUHs
356 corresponding to various saturated states of the watershed, the tension water storage in each grid cell
357 within the basin was considered to be negatively correlated with the Topographic Wetness Index (TWI)
358 (Shi et al., 2008; Tong et al., 2018; Yuan et al., 2019). We assumed topographic information captures
359 the runoff generation heterogeneity at the catchment scale, and the TWI was used as an index to
360 identify rainfall–runoff similarity (Beven and Kirkby, 1979). Areas with similar TWI values are
361 regarded as possessing equal runoff generation potential. Specifically, the areas with larger TWI values
362 tend to be saturated first and contribute to saturation excess rainfall; but the areas with lower TWI
363 values need more water to reach saturation and generate runoff (Gao et al., 2019).

https://doi.org/10.5194/hess-2024-274
Preprint. Discussion started: 23 September 2024

Hydrology and Earth System Sciences
Discussions
Open Access
EGU

Then, the proposed distributed unit hydrographs (DTDUH) are computed based on the saturated areas, which can be expressed by TWI. When calculating discharge using the DTDUH, we should select various DTDUHs based on the time-varying soil moisture within each time interval. Theoretically, the DTDUH is different at each time interval because θ_t is ranging from 0 to 1. However, practically applying time-varying soil moisture based on DTDUH can be a complex task. To improve the effectiveness of the routing method, the soil moisture contents θ_t in Eq. (9) were discretized to 0.25, 0.5, 0.75, and 1 based on the distributions of the TWI. Then, a simplified DTDUH can be obtained in a certain range of soil moisture content. These ranges are presented in Table 3. The distribution of the saturated areas corresponding to different soil proportions is shown in Fig. 6. Similarly, the ratio of excess rainfall intensity and the reference excess rainfall intensity $\frac{I_t}{I_c}$ in Eq. (9) were discretized to 0.5, 1, 1.5, and 2 to improve the calculation efficiency. More details can be found in Yi et al. (2022).

Table 3. The soil moisture content α_t of each interval corresponds to the discrete soil moisture θ_s.

Soil moisture θ_t	$0 \le \theta_t \le 0.25$	$0.25 < \theta_t \le 0.5$	$0.5 < \theta_t \le 0.75$	$0.75 < \theta_t \le 1$
Discrete soil moisture θ_s	0.25	0.5	0.75	1

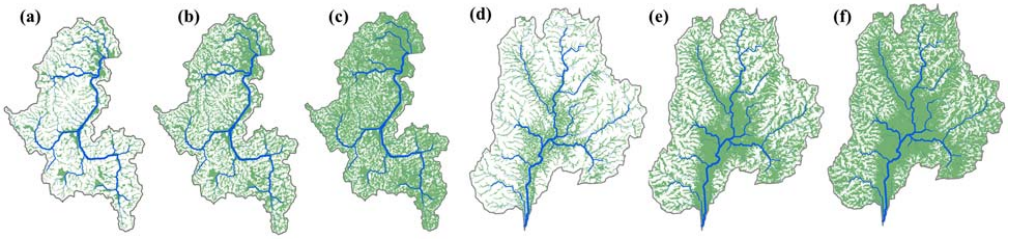

Figure 6. Saturated areas correspond to various soil moisture proportions, where the green area represents the saturated region and the white area represents the unsaturated region. (a), (b) and (c) are the saturated areas corresponding to 0.25, 0.5, and 0.75 soil moisture proportions for the Longhu River

https://doi.org/10.5194/hess-2024-274
Preprint. Discussion started: 23 September 2024

Hydrology and Earth System Sciences
Discussions

381 basin. (d), (e) and (f) are the saturated areas corresponding to 0.25, 0.5, and 0.75 soil moisture
382 proportions for the Dongshi River basin.

383 The computed TDUHs and DTDUHs for the Longhu River basin and the Dongshi River basin
384 are demonstrated in Fig. 7 to Fig. 10. For instance, when the excess rainfall intensities range from 0 to
385 5 mm h^{-1} and the soil moisture contents are between 0 and 0.25, the TDUH used for the surface runoff
386 routing is corresponding to the red line in Fig. 7(a) for the Longhu River basin. Although the time to
387 peak and flow peak discharge can be different for various TDUHs, the areas below the curve are the
388 same as each other. However, the areas below the curve are not necessarily the same for the DTDUH,
389 as the proposed DTDUH is derived from the saturated areas, as shown in Fig. 8. Only when the
390 watershed reaches a global saturated state will the DTDUH be the same as the TDUH.

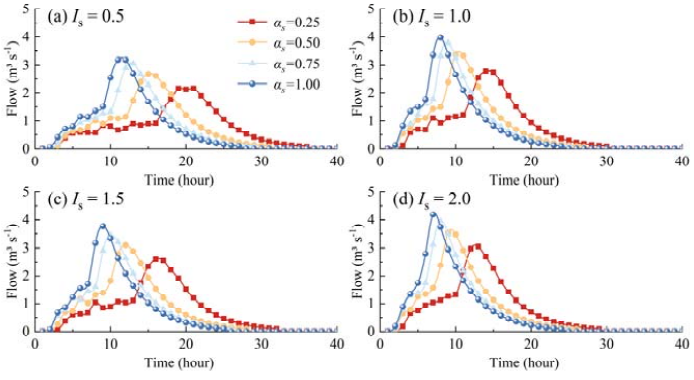

391

392 **Figure 7.** The TDUHs of the Longhu River basin. (a) I_s = 0.5. (b) I_s = 1.0. (c) I_s = 1.5. (d) I_s = 2.0.

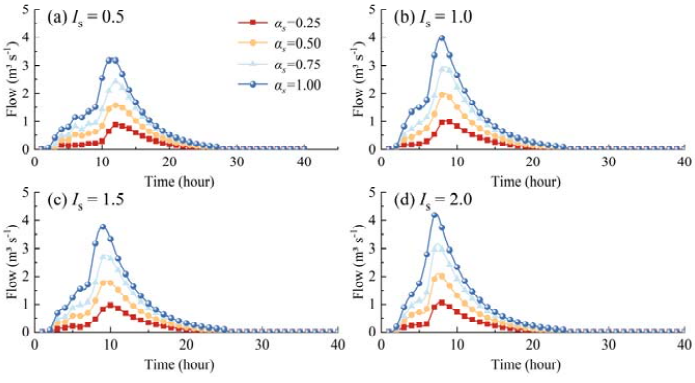

393

https://doi.org/10.5194/hess-2024-274
Preprint. Discussion started: 23 September 2024

Hydrology and Earth System Sciences
Discussions

394 **Figure 8.** The DTDUHs of the Longhu River basin. (a) I_s = 0.5. (b) I_s = 1.0. (c) I_s = 1.5. (d) I_s = 2.0.

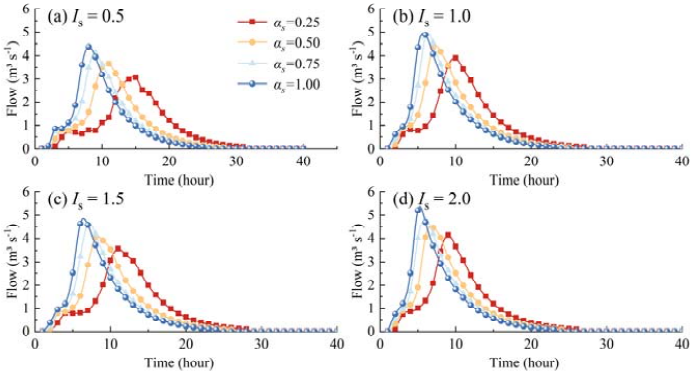

395

396 **Figure 9.** The TDUHs of the Dongshi River basin. (a) I_s = 0.5. (b) I_s = 1.0. (c) I_s = 1.5. (d) I_s = 2.0.

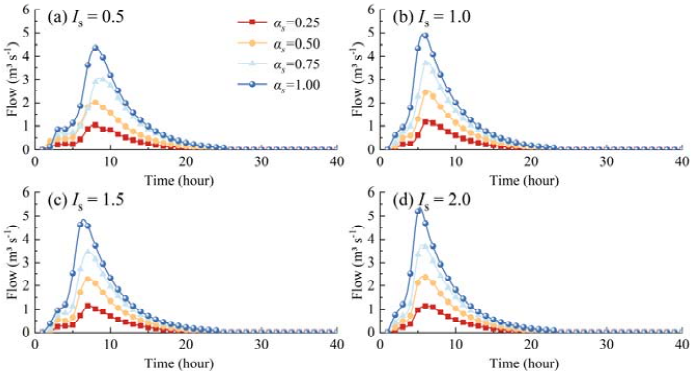

397

398 **Figure 10.** The DTDUHs of the Dongshi River basin. (a) I_s = 0.5. (b) I_s = 1.0. (c) I_s = 1.5. (d) I_s =

399 2.0.

400 It is noteworthy that for the same rainfall intensity, the time to peak of the DTDUHs

401 corresponding to various soil moisture content is almost consistent with slight variations. For instance,

402 the time to peak of DTDUHs presented in Figures 8 and 10 do not vary with the saturation level. This

403 is because we extracted the saturated areas based on the TWI for the DTDUHs, and the derived unit

404 hydrographs correspond only to the saturated areas. To that end, θ_t is almost equal to 1 when deriving

405 DTDUHs, and, as a result, the time to peak varies not very significantly with the soil moisture.

https://doi.org/10.5194/hess-2024-274
Preprint. Discussion started: 23 September 2024

Hydrology and Earth System Sciences
Discussions

4.3 Performances of the DTDUH for the Longhu and Dongshi River basins

We calibrated the three models (XAJ+LR, XAJ+TDUH, and XAJ+DTDUH), respectively, to compare the fluence of heterogeneity of soil moisture on various runoff routing methods. A total of 16 isolated storms with observed runoff responses from 1973 to 2016 were selected to explore the performances of the TDUH and DTDUH for the Longhu River basin. Table 4 lists the E_{NS}, *RMSE*, error of flood peak (Q_p), and error of time to peak (T_p) values for all the models of the Longhu River basin, among which No. 20150831, 20160430, 20160903, and 201651021 are validation datasets. To demonstrate the model performances of different strategies more visually, Fig. 11 shows line charts of the three runoff routing methods for the four indexes in both calibration and validation periods.

Table 4. Calibrated and Validated results of the Longhu River basin.

Flood	E_{NS}			*RMSE* (m³/s)			Q_p			T_p (h)		
events	LR	TDUH	DTDUH	LR	TDUH	DTDUH	LR	TDUH	DTDUH	LR	TDUH	DTDUH
19730508	0.77	0.83	0.85	13.66	11.67	11.11	-0.28	-0.22	-0.21	3	3	3
19730720	0.84	0.87	0.90	22.09	19.85	17.69	-0.22	-0.05	-0.05	1	0	0
19750526	0.60	0.76	0.86	17.04	13.24	10.13	-0.36	-0.27	0.18	0	-1	0
19760702	0.59	0.68	0.67	21.96	19.45	19.73	-0.53	-0.39	-0.39	1	3	3
19770526	0.38	0.11	0.10	21.83	26.09	26.28	-0.30	-0.19	-0.19	3	2	2
19771003	0.54	0.32	0.37	19.29	23.47	22.60	-0.28	-0.20	-0.19	0	3	2
19790607	0.31	0.34	0.47	23.41	22.91	20.39	-0.28	-0.25	-0.25	2	2	2
19890502	0.46	0.49	0.52	28.24	27.65	26.80	-0.64	-0.66	-0.50	-1	1	0
20030517	0.49	0.54	0.54	31.63	30.30	30.07	-0.35	-0.32	-0.32	0	-1	-1
20120527	0.72	0.73	0.72	21.15	20.69	21.03	-0.25	0.03	0.03	-2	0	0
20130713	0.70	0.82	0.81	37.50	28.74	30.22	-0.33	-0.30	-0.32	1	0	0
20150601	0.52	0.84	0.82	19.08	10.94	11.70	0.50	0.15	0.25	0	-1	-1
20150831	0.82	0.74	0.76	11.88	14.12	13.58	-0.21	-0.02	0.00	-3	1	1
20160430	0.93	0.72	0.77	7.33	13.29	13.12	0.01	0.11	0.08	1	1	1
20160903	0.70	0.76	0.81	16.67	13.20	13.75	-0.36	-0.09	-0.04	-4	0	0
20161021	0.73	0.90	0.94	17.22	8.47	8.50	-0.16	0.03	-0.01	-2	-1	-1

https://doi.org/10.5194/hess-2024-274
Preprint. Discussion started: 23 September 2024

Hydrology and Earth System Sciences
Discussions
Open Access
EGU

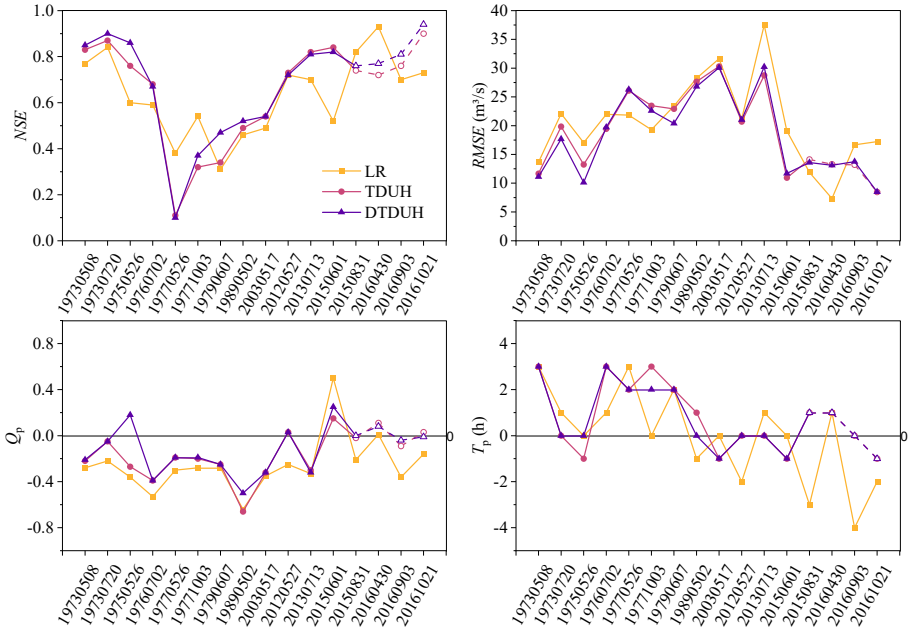

Figure 11. Line chart of the E_{NS}, *RMSE*, Q_p, and T_p for the Longhu River basin.

Results show that TDUH and DTDUH have consistent performances in E_{NS}, *RMSE*, and T_p, and results of the LR method are not stable, sometimes better than that of the DTDUH method, sometimes worse (especially for the criteria Q_p). In the calibration periods, DTDUH performed better than that of TDUH, while in the validation periods, TDUH and DTDUH performed almost consistently. It may be due to the initial conditions of flood events being different from each other. For the calibration periods, the average E_{NS} of the LR, TDUH, and DTDUH methods are 0.58, 0.61 and 0.64, respectively, and 0.80, 0.78, and 0.82 for the validation periods. Simultaneously, the absolute error of the flood peak are 0.36, 0.25, and 0.24 for the calibration periods, respectively, and 0.18, 0.06, and 0.03 for the validation periods. In general, the improvement from the DTDUH is small, and we summarized the possible reasons as follows 1) The surface runoff accounts for 60% ~ 70% of the total runoff, and it is necessary to consider the influence of the heterogeneity of the subsurface stormflow as well as the subsurface

https://doi.org/10.5194/hess-2024-274
Preprint. Discussion started: 23 September 2024

Hydrology and Earth System Sciences
Discussions

429 runoff; 2) the antecedent soil moisture is high, and, thus, the simulation error caused by the spatial
430 heterogeneity of runoff generation is small.

431 Simultaneously, Table 5 lists the E_{NS}, *RMSE*, error of flood peak (Q_p), and error of time to peak
432 (T_p) values for all the models of the Dongshi River basin, among which No. 20190609, 20190612,
433 20200522, and 20200607 are validation dataset. To demonstrate the model performances of different
434 strategies more visually, Fig. 12 shows line charts of the three runoff routing methods for the four
435 indexes in both calibration and validation periods. Compared with the results of Longhu River, the
436 DTDUH, and LR methods showed consistent performances, and were significantly better than the
437 TDUH method. It shows that the DTDUH method shows significant improvement in this basin.

438 **Table 5**. Calibrated and validated results of the Dongshi River basin.

Flood	E_{NS}			*RMSE* (m^3/s)			Q_p			T_p (h)		
events	LR	TDUH	DTDUH	LR	TDUH	DTDUH	LR	TDUH	DTDUH	LR	TDUH	DTDUH
20150509	0.37	0.09	0.32	12.61	15.17	13.08	-0.73	-0.83	-0.76	5	5	5
20150721	0.81	0.87	0.80	11.21	9.25	11.60	0.02	-0.16	0.06	-1	-1	-1
20160811	0.61	0.54	0.67	5.17	5.63	4.78	-0.34	-0.17	-0.38	1	1	1
20160819	0.83	0.68	0.79	2.39	3.34	2.71	-0.26	-0.40	-0.26	0	0	0
20161021	0.93	0.81	0.94	6.99	11.80	6.75	-0.11	-0.27	-0.10	2	5	2
20170501	0.89	0.67	0.86	2.69	4.75	3.11	-0.16	-0.27	0.00	0	1	0
20170515	0.64	0.78	0.64	3.95	3.10	3.97	-0.05	-0.14	-0.07	0	4	4
20170613	0.91	0.76	0.91	8.40	13.48	8.28	-0.26	-0.38	-0.22	2	2	2
20170929	0.75	0.53	0.73	3.71	5.12	3.87	-0.20	-0.21	0.17	-3	2	0
20180606	0.55	0.34	0.53	5.53	6.73	5.68	-0.51	-0.55	-0.55	1	1	1
20180702	0.55	0.59	0.48	4.17	3.96	4.48	-0.51	-0.45	-0.58	2	2	2
20190418	0.61	0.55	0.58	7.54	8.00	7.79	-0.63	-0.67	-0.65	2	12	2
20190609	0.55	0.56	0.75	13.27	13.03	9.83	-0.54	-0.53	-0.42	2	2	2
20190612	0.81	0.76	0.83	4.57	5.09	4.36	-0.18	-0.06	-0.02	0	0	0
20200522	0.77	0.56	0.75	5.24	7.32	5.56	-0.01	-0.02	-0.04	2	2	2
20200607	0.57	0.54	0.61	28.85	30.03	27.54	-0.50	-0.54	-0.50	0	-1	2

https://doi.org/10.5194/hess-2024-274
Preprint. Discussion started: 23 September 2024

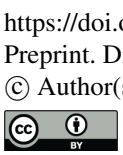

Hydrology and Earth System Sciences
Discussions
Open Access
EGU

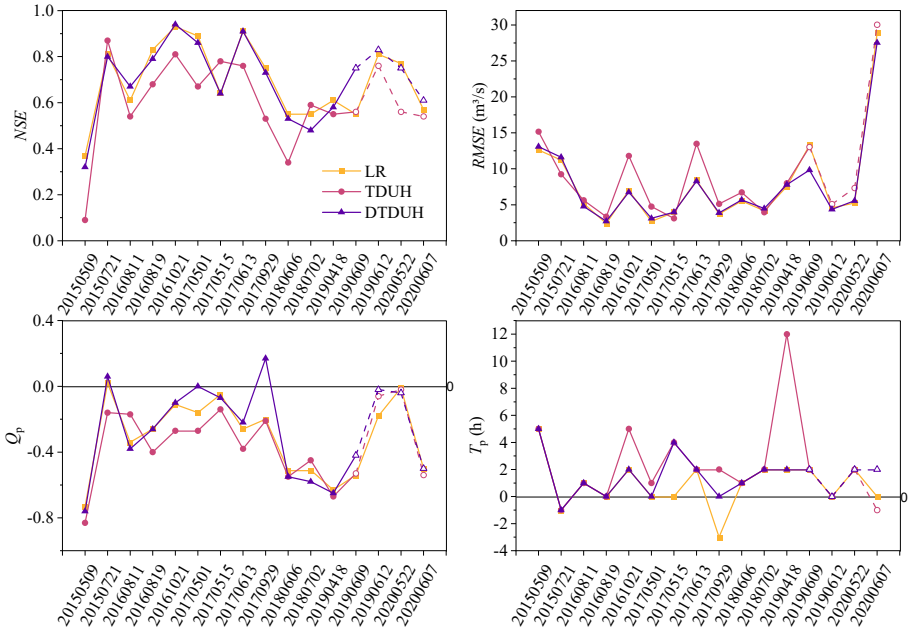

439

440 **Figure 12.** Line chart of the E_{NS}, *RMSE*, Q_p, and T_p for the Dongshi River basin.

441 In addition, we compared the calibrated parameter sets for the two basins, as given in Table 6. It
442 can be found that the parameters of the XAJ model are consistent for three runoff routing methods in
443 the two basins, which means that the derived TDUH and DTDUH are rational. For the Dongshi River
444 basin, the parameters calibrated using DTDUH methods are more consistent with the LR method
445 compared with that of the Longhu River basin, and it revealed that the simulated results using the LR
446 and DTDUH methods could be similar as each other. This conclusion is consistent with the simulation
447 results in Fig. 12, where the LR and DTDUH performed similarly.

448 **Table 6**. Calibrated parameters of the three runoff routing methods for the Longhu and Dongshi River
449 basins

Parameters	Longhu			Dongshi		
	LR	TDUH	DTDUH	LR	TDUH	DTDUH
UM	9.65	7.13	8.29	5.38	8.16	9.13
LM	86.32	85.97	81.23	85.94	66.54	85.21
DM	43.96	47.26	49.25	47.14	28.53	45.65

https://doi.org/10.5194/hess-2024-274
Preprint. Discussion started: 23 September 2024

Hydrology and Earth System Sciences
Discussions

B	0.13	0.39	0.36	0.40	0.40	0.40
IM	0.09	0.10	0.10	0.26	0.02	0.20
KC	0.12	0.80	0.80	1.48	1.50	1.44
C	0.12	0.12	0.12	0.16	0.15	0.12
SM	23.93	33.84	35.98	50.00	50.00	50.00
EX	1.19	1.24	1.10	1.00	1.00	1.00
KI	0.63	0.43	0.41	0.17	0.11	0.13
KG	0.07	0.27	0.29	0.53	0.59	0.57
CI	0.20	0.51	0.56	0.51	0.52	0.49
CG	0.94	0.95	0.94	0.99	0.99	0.99
CS	0.99	-	-	1.00	-	-
L	0.00	0.00	0.00	0.00	0.00	0.00

5. Discussion

5.1 Errors due to spatial scale mismatch between runoff generation and runoff routing

To investigate the possible errors due to spatial scale mismatch between runoff generation and runoff routing, we assumed several sets of excess rainfall with intensities of 5, 10, 15, and 20 mm h^{-1}, and the saturated proportions of the basin are 0.25, 0.5, 0.75 and 1, respectively. Considering the average rainfall intensities of the two basins, the time durations of the rainfall are assumed to change from 1 to 4 h, and the combinations are shown in Table 7.

Table 7. Combinations of the assumed excess rainfall, time duration, and soil moisture content.

Scenario	Depth of excess rainfall (mm)	Time duration (h)	Soil moisture content
1（R-T1-S1）	20（R）	1（T1）	0.25（S1）
2（R-T1-S2）	20（R）	1（T1）	0.50（S2）
3（R-T1-S3）	20（R）	1（T1）	0.75（S3）
4（R-T1-S4）	20（R）	1（T1）	1.00（S4）
5（R-T2-S1）	20（R）	2（T2）	0.25（S1）
6（R-T2-S2）	20（R）	2（T2）	0.50（S2）
7（R-T2-S3）	20（R）	2（T2）	0.75（S3）
8（R-T2-S4）	20（R）	2（T2）	1.00（S4）
9（R-T3-S1）	20（R）	3（T3）	0.25（S1）
10（R-T3-S2）	20（R）	3（T3）	0.50（S2）
11（R-T3-S3）	20（R）	3（T3）	0.75（S3）
12（R-T3-S4）	20（R）	3（T3）	1.00（S4）

https://doi.org/10.5194/hess-2024-274
Preprint. Discussion started: 23 September 2024

13（R-T4-S1）	20（R）	4（T4）	0.25（S1）
14（R-T4-S2）	20（R）	4（T4）	0.50（S2）
15（R-T4-S3）	20（R）	4（T4）	0.75（S3）
16（R-T4-S4）	20（R）	4（T4）	1.00（S4）

458 Thus, 16 combinations can be formed based on Table 7. For example, combination R-T1-S1
459 indicates there is a total depth of 20 mm excess rainfall in the global watershed with the time duration
460 being 1 hour (20 mm h^{-1}), and the saturated proportion of the basin is 0.25. Similarly, combination R-
461 T3-S2 indicates there is a total depth of 20 mm excess rainfall in the global watershed with the time
462 durations being 4 hours (5 mm h^{-1}), and the saturated proportion of the basin is 0.50. Then, the flow
463 hydrograph due to the assumed excess rainfall can be obtained using the TDUH and the DTDUH, thus
464 comparing the errors of spatial scale mismatch between runoff generation and runoff routing. The flow
465 hydrograph computed using the TDUH and DTDUH corresponding to the two basins is shown in Fig.
466 13 and Fig. 14, respectively.

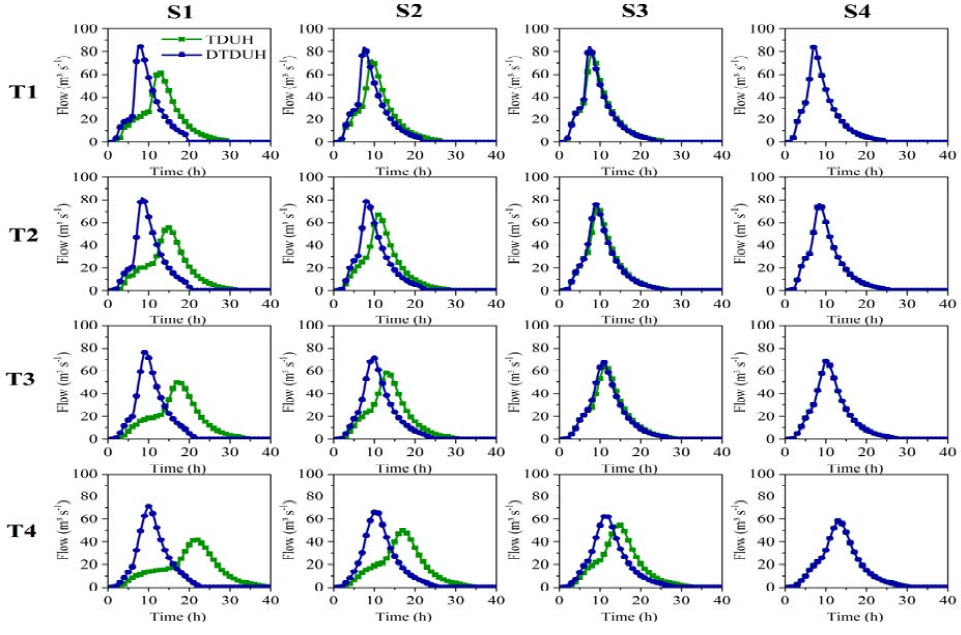

467

468 **Figure 13.** Errors in the flow hydrograph due to spatial mismatch between runoff generation and runoff

https://doi.org/10.5194/hess-2024-274
Preprint. Discussion started: 23 September 2024

Hydrology and Earth System Sciences
Discussions

469 routing for the Longhu River basin

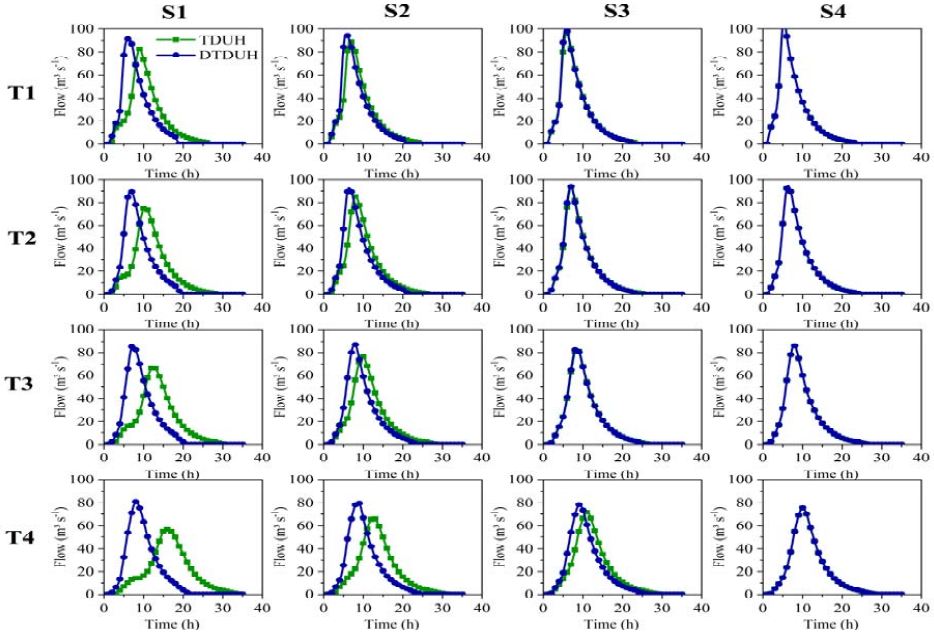

470

471 **Figure 14.** Errors in the flow hydrograph due to spatial mismatch between runoff generation and runoff
472 routing for the Dongshi River basin.

473 It can be found from Fig. 13 that the soil moisture significantly influences the results of the TDUH,
474 while the results of the DTDUH are almost not changed with the variation of soil moisture for the
475 Longhu River basin. When the saturated soil moisture proportion is low, the results of the two routing
476 methods are significantly different. Simultaneously, when the saturated soil moisture proportion
477 exceeds 0.5, the results of the TDUH and the DTDUH perform almost consistently. The differences
478 between the results of the two methods increase with the duration of excess rainfall.

479 For the Dongshi River basin, it can be seen from Fig. 14 that patterns of the soil moisture and
480 time duration on the performances are consistent with those of the Longhu River basin. Conversely,
481 the soil moisture shows a more pronounced effect on the DTDUH, and the flow peak discharge

https://doi.org/10.5194/hess-2024-274
Preprint. Discussion started: 23 September 2024


Hydrology and Earth System Sciences
Discussions

482 becomes higher with the soil moisture changing from S1 to S4. It can also be found that the differences
483 between the results of the TDUH and the DTDUH in the Dongshi River basin are also significant, but
484 show more limited for the Dongshi River basin than that of the Longhu River basin.

485 In summary, the performances of the TDUH and DTDUH are consistent for higher soil moisture
486 and higher rainfall intensity. When the soil moisture is low and the time duration of the excess rainfall
487 is long, we should pay much attention to the errors due to the spatial scale mismatch between runoff
488 generation and runoff routing. Additionally, the differences caused by this mismatch vary significantly
489 in different watersheds.

490 *5.2 Advantages and limitations of the proposed DTDUH*

491 Based on the analysis of Sections 4.3 and 5.2, we found that the accuracy of DTDUHs varies in
492 different basins, specifically, performances of the DTDUH in the Longhu basin are more similar to
493 that of the TDUHs, while the simulation results in the Dongshi basin are more consistent with that of
494 the LR method. In general, the DTDUHs performed the best over the three runoff routing methods for
495 both test cases. There are many reasons why DTDUH simulation is superior than others, and we
496 summarized the main differences between TDUH and DTDUHs, including their definition and
497 assumptions. The DTDUH was defined as a typical hydrograph of direct runoff which gets generated
498 from one centimeter of effective rainfall falling at a uniform rate over the saturated drainage basin
499 uniformly during a specific duration. This realization was significantly different from the
500 understandings of Sherman (1932), who defined the unit hydrograph of a watershed as a direct runoff
501 hydrograph that results from 10 mm of excess rainfall that is generated uniformly over the drainage
502 area at a constant rate for an effective duration. The proposed DTDUH was computed based on the

https://doi.org/10.5194/hess-2024-274
Preprint. Discussion started: 23 September 2024

Hydrology and Earth System Sciences
Discussions

503 runoff generation areas instead of the whole basin, and this is the main advantage of DTDUH over
504 TDUHs. Simultaneously, the assumption of the DTDUH remained unchanged as the traditional unit
505 hydrograph, such as a spatially uniform distributed effective precipitation. Some researchers also did
506 similar research. For example, Andrieu et al. (2021) proposed an Event-specific Geomorphological
507 Instantaneous Unit Hydrograph (E-GIUH), and the method relies on the width function-based GIUH
508 (Rigon et al., 2016), as adapted to take into account the spatial variability of rainfall through replacing
509 the width function by the rainfall width function.

510 Although DTDUH showed advantages in both basins, the degree of improvement compared with
511 TDUH was not consistent. Therefore, we summarized the potential limitations of the DTDUH. First,
512 we utilized the DTDUH only for the surface runoff in both basins, proportions of the subsurface storm
513 flow and subsurface runoff may cause considerable interference to the simulation results. Runoff
514 components of the Longhu and Dongshi River basins are given in Fig. 15.

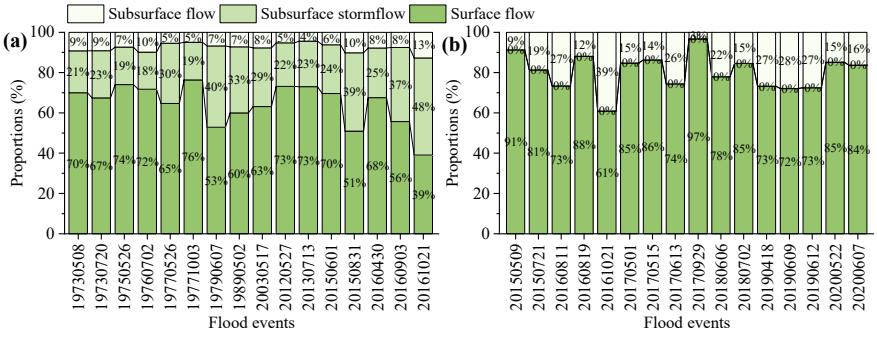

515

516 **Figure 15.** Details of the runoff components of the 16 flood events for the (a) Longhu River basin. (b)
517 Dongshi River basin.

518 Fig. 15 shows that the average surface runoff ratio in Longhu basin and Dongshi basin is 64.4%
519 and 80.3%, respectively. This result suggested that the improvement in accuracy caused by DTDUH

https://doi.org/10.5194/hess-2024-274
Preprint. Discussion started: 23 September 2024

Hydrology and Earth System Sciences
Discussions

520 may be more significant in the Dongshi basin. And, this conclusion is consistent with the calibration
521 and verification results in Section 4.3. Second, a hybrid runoff generation process pattern formed by
522 more than one mechanism can often be identified in semi-humid, semi-arid, and mountain watersheds,
523 because of the heterogeneity of underlying surface conditions and meteorological factors (Hu et al.,
524 2021; Yi et al., 2023). When there occurs more than the saturation-excess rainfall, the saturated area
525 extraction method based on the TWI will not be applicable as the excess rainfall can also be generated
526 from the unsaturated areas.

527 Fig. 16 shows the antecedent soil moisture conditions for the Longhu and Dongshi River basins.
528 It can be found that the antecedent soil moisture can be low for some flood events, such as No.
529 19790607, 19890502, 20150509, and so on. When the antecedent soil moisture is low and the rainfall
530 intensity is high, the drainage basin may produce not only the saturation excess, which results in low
531 accuracy of the DTDUH method.

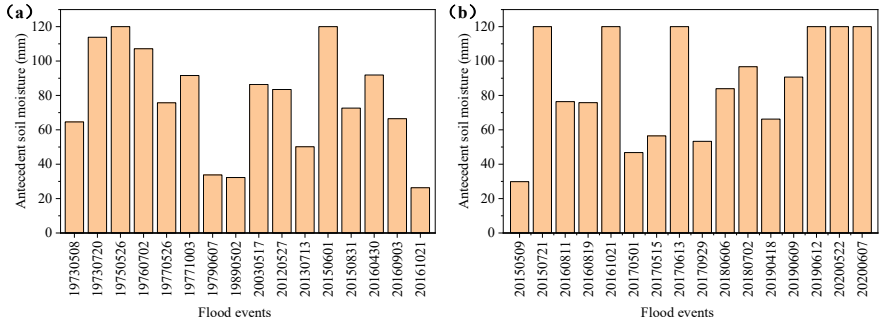

532

533 **Figure 16.** Details of the antecedent soil moisture of the 16 flood events for the (a) Longhu River basin.
534 (b) Dongshi River basin.

https://doi.org/10.5194/hess-2024-274
Preprint. Discussion started: 23 September 2024


Hydrology and Earth System Sciences
Discussions

6. Conclusions

A novel DTDUH method was proposed to explore the influence of spatial heterogeneity of runoff generation on the runoff routing. The XAJ model was used as the hydrological modeling framework. The Longhu River basin and the Dongshi River basin were selected as two case studies. The results of the three surface runoff routing methods including the linear reservoir, TDUH, and DTDUH were compared. The advantages and shortcomings of the proposed method have been discussed. The main conclusions can be summarized as follows:

1. A novel DTDUH method designed for surface runoff routing was proposed based on the TDUH method. The traditional TDUH method was derived based on the whole basin, and the proposed method was designed only for the saturated areas. The DTDUH method considered not only the time-varying rainfall intensities and soil moisture, but also the time-varying saturated areas of the watershed which were extracted based on the TWI.

2. The rationality of the proposed method was verified by comparing the performances of XAJ+LR, XAJ + TDUH, and XAJ +DTDUH models, which were calibrated separately. Results show that the proposed method exhibited consistent or better performance compared with that of the LR routing method, and performed better than the TDUH method.

3. The influence of spatial heterogeneity of runoff generation on the runoff routing was carried out by comparing the performances of the TDUH and the DTDUH. Results show that the heterogeneity of runoff generation can be significantly different in different basins. Simultaneously, the heterogeneity of various runoff components is supposed to be considered.

https://doi.org/10.5194/hess-2024-274
Preprint. Discussion started: 23 September 2024


Hydrology and Earth System Sciences
Discussions

Data availability

Due to the strict security requirements from the departments, some or all data, models, or code generated or used in the study are proprietary or confidential in nature and may only be provided with restrictions (e.g. anonymized data).

Author contributions

Bin Yi conceived the original idea, designed the methodology, developed the code, and performed the study. Lu Chen, Bin Yi, Binlin Yang, Zhiyuan Leng, Siming Li, and Tao Xie contributed to the interpretation of the results. Bin Yi wrote the paper, and Lu Chen revised the paper.

Competing interests

The authors declare that they have no conflict of interest.

Acknowledgments

This study was financially supported by the National Key R&D Program of China (2023YFC3081000, 2021YFC3200400), and the Science and Technology Plan Projects of Tibet Autonomous Region (XZ202301YD0044C).

References

Ajward, M. H., Muzik, I., 2000. A spatially varied unit hydrograph model. Journal of Environmental Hydrology, 8(7).

Andrieu, H., Moussa, R., Kirstetter, P.-E., 2021. The Event-specific Geomorphological Instantaneous Unit Hydrograph (E-GIUH): The basin hydrological response characteristic of a flood event. Journal of Hydrology, 603: 127158. https://doi.org/10.1016/j.jhydrol.2021.127158.

Beven, K. J., Kirkby, M. J., 1979. A physically based, variable contributing area model of basin hydrology / Un modèle à base physique de zone d'appel variable de l'hydrologie du bassin versant. Hydrological Sciences Bulletin, 24(1): 43-69. https://doi.org/10.1080/02626667909491834.

https://doi.org/10.5194/hess-2024-274
Preprint. Discussion started: 23 September 2024

581 Boughton, W., 2004. The Australian water balance model. Environmental Modelling &
582 Software, 19(10): 943-956. https://doi.org/10.1016/j.envsoft.2003.10.007.
583 Brunner, M. I., Swain, D. L., Wood, R. R., Willkofer, F., Done, J. M., Gilleland, E.,
584 Ludwig, R., 2021. An extremeness threshold determines the regional response
585 of floods to changes in rainfall extremes. Communications Earth &
586 Environment, 2(1): 173. https://doi.org/10.1038/s43247-021-00248-x.
587 Bunster, T., Gironás, J., Niemann, J. D., 2019. On the influence of upstream flow
588 contributions on the basin response function for hydrograph prediction. Water
589 Resources Research, 55(6): 4915-4935.
590 https://doi.org/10.1029/2018WR024510.
591 Cho, Y., Engel, B. A., Merwade, V. M., 2018. A spatially distributed Clark's unit
592 hydrograph based hybrid hydrologic model (Distributed-Clark). Hydrological
593 Sciences Journal, 63(10): 1519-1539.
594 https://doi.org/10.1080/02626667.2018.1516042.
595 Clark, C. O., 1945. Storage and the Unit Hydrograph. Transactions of the American
596 Society of Civil Engineers, 110(1): 1419-1446.
597 https://doi.org/10.1061/TACEAT.0005800.
598 Czyzyk, K., Mirossi, D., Abdoulhak, A., Hassani, S., Niemann, J. D., Gironás, J., 2020.
599 Impacts of Channel Network Type on the Unit Hydrograph. Water, 12(3): 669.
600 https://doi.org/10.3390/w12030669.
601 Du, J., Xie, H., Hu, Y., Xu, Y., Xu, C.-Y., 2009. Development and testing of a new storm
602 runoff routing approach based on time variant spatially distributed travel time
603 method. Journal of Hydrology, 369(1-2): 44-54.
604 https://doi.org/10.1016/j.jhydrol.2009.02.033.
605 Duan, Q., Sorooshian, S., Gupta, V., 1992. Effective and efficient global optimization
606 for conceptual rainfall - runoff models. Water Resources Research, 28(4):
607 1015-1031. https://doi.org/10.1029/91WR02985.
608 Foda, R. F., Awadallah, A. G., Gad, M. A., 2017. A Fast Semi Distributed Rainfall
609 Runoff Model for Engineering Applications in Arid and Semi-Arid Regions.
610 Water Resources Management, 31(15): 4941-4955.
611 https://doi.org/10.1007/s11269-017-1787-2.
612 Gao, H., Birkel, C., Hrachowitz, M., Tetzlaff, D., Soulsby, C., Savenije, H. H. G., 2019.
613 A simple topography-driven and calibration-free runoff generation module.
614 Hydrology and Earth System Sciences, 23(2): 787-809. 10.5194/hess-23-787-
615 2019.
616 Gibbs, M., Dandy, G., Maier, H., 2010. Evaluation of parameter setting for two GIS
617 based unit hydrograph models. Journal of Hydrology, 393(3-4): 197-205.
618 https://doi.org/10.1016/j.jhydrol.2010.08.014.
619 Goñi, M., López, J. J., Gimena, F. N., 2019. Geomorphological instantaneous unit
620 hydrograph model with distributed rainfall. CATENA, 172: 40-53.
621 https://doi.org/10.1016/j.catena.2018.08.010.
622 Goodrich, D. C., Lane, L. J., Shillito, R. M., Miller, S. N., Syed, K. H., Woolhiser, D.

https://doi.org/10.5194/hess-2024-274
Preprint. Discussion started: 23 September 2024

A., 1997. Linearity of basin response as a function of scale in a semiarid watershed. Water Resources Research, 33(12): 2951-2965. https://doi.org/10.1029/97WR01422.

Gray, D. M., 1961. Synthetic Unit Hydrographs for Small Watersheds. Journal of the Hydraulics Division, 87(4): 33-54. https://doi.org/10.1061/JYCEAJ.0000631.

Grimaldi, S., Petroselli, A., Alonso, G., Nardi, F., 2010. Flow time estimation with spatially variable hillslope velocity in ungauged basins. Advances in Water Resources, 33(10): 1216-1223. https://doi.org/10.1016/j.advwatres.2010.06.003.

Grimaldi, S., Petroselli, A., Nardi, F., 2012. A parsimonious geomorphological unit hydrograph for rainfall–runoff modelling in small ungauged basins. Hydrological Sciences Journal, 57(1): 73-83. https://doi.org/10.1080/02626667.2011.636045.

Gupta, V. K., Waymire, E., Wang, C. T., 1980. A representation of an instantaneous unit hydrograph from geomorphology. Water Resources Research, 16(5): 855-862. https://doi.org/10.1029/WR016i005p00855.

Hoang, L., Schneiderman, E. M., Moore, K. E. B., Mukundan, R., Owens, E. M., Steenhuis, T. S., 2017. Predicting saturation-excess runoff distribution with a lumped hillslope model: SWAT-HS. Hydrological Processes, 31(12): 2226-2243. https://doi.org/10.1002/hyp.11179.

Hu, C. H., Ran, G., Li, G., Yu, Y., Wu, Q., Yan, D. H., Jian, S. Q., 2021. The effects of rainfall characteristics and land use and cover change on runoff in the Yellow River basin, China. Journal of Hydrology and Hydromechanics, 69(1): 29-40. https://doi.org/10.2478/johh-2020-0042.

Huang, Q., Qin, G., Zhang, Y., Tang, Q., Liu, C., Xia, J., Chiew, F. H. S., Post, D., 2020. Using Remote Sensing Data-Based Hydrological Model Calibrations for Predicting Runoff in Ungauged or Poorly Gauged Catchments. Water Resources Research, 56(8): e2020WR028205. https://doi.org/10.1029/2020WR028205.

Kirkby, M. J., 1976. Tests of the random network model, and its application to basin hydrology. Earth Surface Processes, 1(3): 197-212. https://doi.org/10.1002/esp.3290010302.

Lee, K. T., Chen, N.-C., Chung, Y.-R., 2008. Derivation of variable IUH corresponding to time-varying rainfall intensity during storms/Dérivation d'un HUI variable correspondant à l'évolution temporelle de l'intensité pluviométrique durant les averses. Hydrological Sciences Journal, 53(2): 323-337. https://doi.org/10.1623/hysj.53.2.323.

Li, H. Y., Sivapalan, M., 2014. Functional approach to exploring climatic and landscape controls on runoff generation: 2 Timing of runoff storm response. Water Resources Research, 50(12): 9323-9342. https://doi.org/10.1002/2014wr016308.

Liang, X., Lettenmaier, D. P., Wood, E. F., Burges, S. J., 1994. A simple hydrologically based model of land surface water and energy fluxes for general circulation

https://doi.org/10.5194/hess-2024-274
Preprint. Discussion started: 23 September 2024

models. Journal of Geophysical Research: Atmospheres, 99(D7): 14415-14428. https://doi.org/10.1029/94JD00483.

Maidment, D. R., Olivera, F., Calver, A., Eatherall, A., Fraczek, W., 1996. Unit Hydrograph Derived from a Spatially Distributed Velocity Field. Hydrological Processes, 10(6): 831-844. https://doi.org/10.1002/(SICI)1099-1085(199606)10:6<831::AID-HYP374>3.0.CO;2-N.

Martinez, V., Garcia, A., Ayuga, F., 2002. Distributed routing techniques developed on GIS for generating synthetic unit hydrographs. Transactions of the ASAE, 45(6): 1825. https://doi.org/10.13031/2013.11433.

Melesse, A. M., Graham, W. D., 2004. Storm runoff prediction based on a spatially distributed travel time method utilizing remote sensing and GIS. Journal of the American Water Resources Association, 40(4): 863-879. https://doi.org/10.1111/j.1752-1688.2004.tb01051.x.

Minshall, N. E., 1960. Predicting storm runoff on small experimental watersheds. Journal of the Hydraulics Division, 86(8): 17-38

Monajemi, P., Khaleghi, S., Maleki, S., 2021. Derivation of instantaneous unit hydrographs using linear reservoir models. Hydrology Research, 52(2): 339-355. https://doi.org/10.2166/nh.2021.171.

Moore, R. J., 2007. The PDM rainfall-runoff model. Hydrol. Earth Syst. Sci., 11(1): 483-499. https://doi.org/10.5194/hess-11-483-2007.

Noto, L. V., La Loggia, G., 2007. Derivation of a distributed unit hydrograph integrating GIS and remote sensing. Journal of Hydrologic Engineering, 12(6): 639-650. https://doi.org/10.1061/(Asce)1084-0699(2007)12:6(639).

Paul, P. K., Kumari, N., Panigrahi, N., Mishra, A., Singh, R., 2018. Implementation of cell-to-cell routing scheme in a large scale conceptual hydrological model. Environmental Modelling & Software, 101: 23-33. https://doi.org/10.1016/j.envsoft.2017.12.003.

Rigon, R., Bancheri, M., Formetta, G., De Lavenne, A., 2016. The geomorphological unit hydrograph from a historical - critical perspective. Earth Surface Processes Landforms, 41(1): 27-37. https://doi.org/10.1002/esp.3855.

Rodríguez-Iturbe, I., González-Sanabria, M., Bras, R. L., 1982. A geomorphoclimatic theory of the instantaneous unit hydrograph. Water Resources Research, 18(4): 877-886. https://doi.org/10.1029/WR018i004p00877.

Rodríguez-Iturbe, I., Valdés, J. B., 1979. The geomorphologic structure of hydrologic response. Water Resources Research, 15(6): 1409-1420. https://doi.org/10.1029/WR015i006p01409.

Rodríguez-Iturbe, I., Ijjász-Vásquez, E. J., Bras, R. L., & Tarboton, D. G., 1992. Power law distributions of discharge mass and energy in river basins. Water Resources Research, 28(4), 1089– 1093. https://doi.org/10.1029/91WR03033.

Sherman, L. K.: Streamflow from rainfall by the unit-graph method, Eng. News-Rec., 108:501-505, 1932.

Sarangi, A., Madramootoo, C. A., Enright, P., Prasher, S. O., 2007. Evaluation of three

https://doi.org/10.5194/hess-2024-274
Preprint. Discussion started: 23 September 2024

Hydrology and Earth System Sciences
Discussions

unit hydrograph models to predict the surface runoff from a Canadian watershed. Water Resources Management, 21(7): 1127-1143. https://doi.org/10.1007/s11269-006-9072-9.

Seo, Y., Park, S. Y., Schmidt, A. R., 2016. Implication of the flow resistance formulae on the prediction of flood wave propagation. Hydrological Sciences Journal, 61(4): 683-695. https://doi.org/10.1080/02626667.2014.992787.

Shi, P., Rui, X. F., Qu, S. M., Chen, X., 2008. Calculating storage capacity with topographic index. Advances in Water Science, 19(2): 264-267

Snyder, F. F., 1938. Synthetic unit-graphs. Eos, Transactions American Geophysical Union, 19(1): 447-454. https://doi.org/10.1029/TR019i001p00447.

Tong, B., Li, Z., Yao, C., Wang, J., Huang, Y., 2018. Derivation of the Spatial Distribution of Free Water Storage Capacity Based on Topographic Index. Water, 10(10): 1407. https://doi.org/10.3390/w10101407.

Tromp-Van Meerveld, H. J., Mcdonnell, J. J., 2006. Threshold relations in subsurface stormflow: 1. A 147-storm analysis of the Panola hillslope. Water Resources Research, 42(2): W02411. https://doi.org/10.1029/2004wr003778.

Yi, B., Chen, L., 2022. A time-varying distributed unit hydrograph method considering dynamic flow routing path. Advances in Water Science, 33(6): 944-954. https://doi.org/10.14042/j.cnki.32.1309.2022.06.009.

Yi, B., Chen, L., Liu, Y., Guo, H., Leng, Z., Gan, X., Xie, T., Mei, Z., 2023. Hydrological modelling with an improved flexible hybrid runoff generation strategy. Journal of Hydrology, 620: 129457. https://doi.org/10.1016/j.jhydrol.2023.129457.

Yi, B., Chen, L., Zhang, H., Singh, V. P., Jiang, P., Liu, Y., Guo, H., Qiu, H., 2022. A time-varying distributed unit hydrograph method considering soil moisture. Hydrology and Earth System Sciences, 26(20): 5269-5289. https://doi.org/10.5194/hess-26-5269-2022.

Yuan, F., Zhang, L., Soe, K. M., Ren, L., Zhao, C., Zhu, Y., Jiang, S., Liu, Y., 2019. Applications of TRMM- and GPM-Era Multiple-Satellite Precipitation Products for Flood Simulations at Sub-Daily Scales in a Sparsely Gauged Watershed in Myanmar. Remote Sensing, 11(2): 140. https://doi.org/10.3390/rs11020140.

Zhao, R. J., 1992. The Xinanjiang model applied in China. Journal of Hydrology, 135(1): 371-381. https://doi.org/10.1016/0022-1694(92)90096-E.

Zhao, R. J., Zuang, Y. L., Fang, L. R., Liu, X. R., 1980. The Xinanjiang model[C]//Proceedings of the Oxford Symposium: 351-356. https://doi.org/10.1016/0022-1694(92)90096-E.

Zhou, Q., Chen, L., Singh, V. P., Zhou, J., Chen, X., Xiong, L., 2019. Rainfall-runoff simulation in karst dominated areas based on a coupled conceptual hydrological model. Journal of Hydrology, 573: 524-533. https://doi.org/10.1016/j.jhydrol.2019.03.099.